IET Power Electronics

Research Article

ISSN 1755-4535
Received on 7th May 2014
Accepted on 15th November 2014
doi: 10.1049/iet-pel.2014.0373
www.ietdl.org

Analysis, control and experimental verification of a single-phase capacitive-coupling grid-connected inverter

Ning-Yi Dai[1] ✉, *Wen-Chen Zhang*[1], *Man-Chung Wong*[1], *Josep M. Guerrero*[2], *Chi-Seng Lam*[1,3]

[1]*Electrical and Computer Engineering Department, University of Macau, Macao, People's Republic of China*
[2]*Department of Energy Technology, Aalborg University, Denmark*
[3]*State Key Laboratory of Analog and Mixed-Signal VLSI, University of Macau, Macao, People's Republic of China*
✉ *E-mail: nydai@umac.mo*

Abstract: This study proposes a capacitive-coupling grid-connected inverter (CGCI), which consists of a full-bridge single-phase inverter coupled to a power grid via one capacitor in series with an inductor. The fundamental-frequency impedance of the coupling branch is capacitive. In contrast with the conventional inductive-coupling grid-connected inverter (IGCI), this structure provides an alternative interface for use between a low-voltage DC microgrid and an AC grid. A comparison between the CGCI and the IGCI is performed. It is concluded that the CGCI is able to transfer active power and provide lagging reactive power at an operational voltage much lower than that of the IGCI. This reduces the system's initial cost and operational losses, as well as the energy stored in the DC-link capacitor. The CGCI has been analysed and a DC voltage selection method is proposed. Using this method, the DC-link voltage of the CGCI remains at approximately of 50% of the peak grid voltage. In addition, a *P*-unit current controller is proposed for use with the CGCI, as a proportional–integral controller is not suitable. Finally, simulation and experiments show the effectiveness of the proposed approach.

1 Introduction

Owing to increasing concern for the environment, interest in renewable energy resources has intensified. Distributed generation based on renewable green energy is expected to increase at an unprecedented rate worldwide [1–3]. The energy obtained from renewable sources is not only used to feed local loads but is also transferred to the grid. Grid-connected inverters provide flexible interfaces for the importation and exportation of renewable energy to and from the grid [4–7].

In the past, the main task of a grid-connected inverter was to transfer active power from renewable energy resources to the grid [8–10]. However, the integration of uncontrollable resources, such as wind and solar energy, may endanger the stability and power quality of the grid. Independent reactive power compensation devices such as active power filters or static synchronous compensators can be installed to ensure that the chief task of a grid-connected inverter is active-power flow control [11–13].

As the current of an active-power flow is orthogonal to that of a reactive power flow, it is economical to use the same inverter to transfer active and reactive power. Inverters capable of providing reactive power to the utility grid played a very important role in today's systems. Controlling reactive power improves the quality of low/medium voltage distribution networks, ensuring that the latest technical requirements set by distribution system operators can be met [14, 15]. Parallel-connected inverters with active and reactive power flow control have been examined by the authors [16–19]. Systems that integrate renewable energy sources and provide wide-range power flow control have been investigated by the authors [20–24]. However, grid-connected inverters capable of wide-range reactive power control has a high direct current (DC)-link voltage, as the voltage drop on the coupling inductor is proportional to the reactive power [23, 24]. In [20], two auxiliary inverters are added to increase the output voltage range of a grid-connected inverter. To provide wide-range reactive power control, a grid-connected inverter must have a high rating, which requires a lot of energy to be stored in high-voltage DC-link capacitors [25, 26]. This increases the system's cost and operational losses.

A parallel-connected inverter used to integrate a microgrid or renewable energy source into the utility grid, as described above, is usually coupled to the point of common coupling (PCC) via an inductor, an inductor–capacitor (LC) filter or an LCL filter. Therefore such parallel-connected inverters are classified as inductive-coupling grid-connected inverters (IGCIs) in this paper. Another type of parallel-connected inverter, which is coupled to the PCC via one capacitor in series with an inductor, has been used in reactive power compensation and harmonic suppression devices [27, 28]. The equivalent impedance of the coupling branch at a fundamental-frequency is capacitive. Therefore this type of inverter is classified as a capacitive-coupling grid-connected inverter (CGCI). The existing literature has shown that the rating of a power converter is reduced when capacitors are inserted into its coupling branch [29, 30]. Capacitor banks are usually much cheaper per KVA than active power filters from the same vendor [31–33]. Therefore, CGCIs provide a more cost-effective solution than IGCIs, particularly when used to suppress the reactive power of high-power loads.

The active power transfer capability of CGCIs was first examined by Zhang *et al.* [29], which showed that a CGCI is able to transfer active power and compensate reactive power when its operational voltage is lower than the grid voltage. However, the study used a fixed injected current to compare the CGCI with an IGCI and did not compare the power transfer capability of the two devices at different power levels. In addition, Zhang *et al.* [29] did not discuss DC-voltage selection for the CGCI. Previous work has shown that CGCIs are able to compensate harmonic currents at a low operational voltage by tuning coupling impedance [27, 34]. As the focus of this paper is power flow control at the fundamental frequency, the design and control of the CGCIs with harmonic suppression capability is not addressed.

In Section 2, the power flow control characteristics of an IGCI and a CGCI are analysed and compared, with special reference to the relationship between the operational voltage and the controllable power range. In Section 3, the power control capability of the

proposed CGCI and the DC voltage selection method are described. A control system block diagram is provided and analysed in Section 4. In Section 5, the results of simulations are shown to verify the effectiveness of the proposed CGCI. The experimental results are provided in Section 6.

2 Comparison of IGCI and CGCI

The configuration of a single-phase IGCI is shown in Fig. 1*a*. A CGCI can be created from a single-phase IGCI by replacing the coupling inductor with a capacitor in series with an inductor, as shown in Fig. 1*b*. The power flow control characteristics of the two inverters are compared in this section. It is assumed that the DC bus of each inverter receives active power from an external source, which may be a renewable energy source or an energy storage unit.

The IGCI is coupled to the grid via an inductor, which is mainly used to suppress output current ripples. The CGCI is coupled to the grid via an LC branch, which presents a capacitive impedance at the fundamental frequency. The LC branch can be replaced by a capacitor in an equivalent circuit. The impedance of the coupling branch is expressed as follows

$$X_c = Z\angle\theta = -j\frac{1}{\omega C_C} + j\omega L_C = -j\frac{1}{\omega C} \tag{1}$$

It is assumed that the voltage V_s at the PCC is located on the positive horizontal axis and has a phase angle of zero. The current injected from the IGCI and the CGCI to the power grid is expressed as follows

$$I_c = I_{c\cdot d} + jI_{c\cdot q} \tag{2}$$

The complex power flowing from the inverter to the grid is expressed as follows

$$\tilde{S} = \vec{U}\cdot\overrightarrow{I^*} = V_s\cdot\left(I_{c\cdot d} - jI_{c\cdot q}\right) = P_{inj} + Q_{inj} \tag{3}$$

According to the direction of the current defined in Fig. 1, P_{inj} is positive when active power is injected into the grid, and Q_{inj} is positive when the reactive current lags the grid-side voltage, that is, reactive power is provided to compensate for the inductive loads. When only the fundamental-frequency component is considered, meaning that the harmonic components are ignored, the grid-connected inverter is modelled as a voltage source. The power flow between the inverter and the grid can be calculated as shown below, following [35, 36]

$$P_{inj} = \left(\frac{V_s V_{inv}}{Z}\cos\delta - \frac{V_s^2}{Z}\right)\cos\theta + \frac{V_s V_{inv}}{Z}\sin\delta\cdot\sin\theta \tag{4}$$

$$Q_{inj} = \left(\frac{V_s V_{inv}}{Z}\cos\delta - \frac{V_s^2}{Z}\right)\sin\theta - \frac{V_s V_{inv}}{Z}\sin\delta\cdot\cos\theta \tag{5}$$

In (4) and (5), V_{inv} is the output voltage of the inverter; and δ represents the phase angle between V_s and V_{inv}. Table 1 provides the Z and θ values for the IGCI and the CGCI. The power base is defined for the IGCI and the CGCI, respectively. The expressions

Table 1 Power base and power flow in per-unit form

	IGCI	CGCI
coupling impedance	$Z=\omega L$, $\theta=90°$	$Z=1/(\omega C)$, $\theta=-90°$
power base	$S_{base\_i}=V_s^2/(\omega L)$	$S_{base\_c}=V_s^2\cdot\omega C$
active power	$\frac{P_{inj}}{S_{base\_i}}=\frac{V_{inv\_i}}{V_s}\sin\delta$	$\frac{P_{inj}}{S_{base\_c}}=-\frac{V_{inv\_c}}{V_s}\sin\delta$
reactive power	$\frac{Q_{inj}}{S_{base\_i}}=\frac{V_{inv\_i}}{V_s}\cos\delta-1$	$\frac{Q_{inj}}{S_{base\_c}}=1-\frac{V_{inv\_c}}{V_s}\cos\delta$

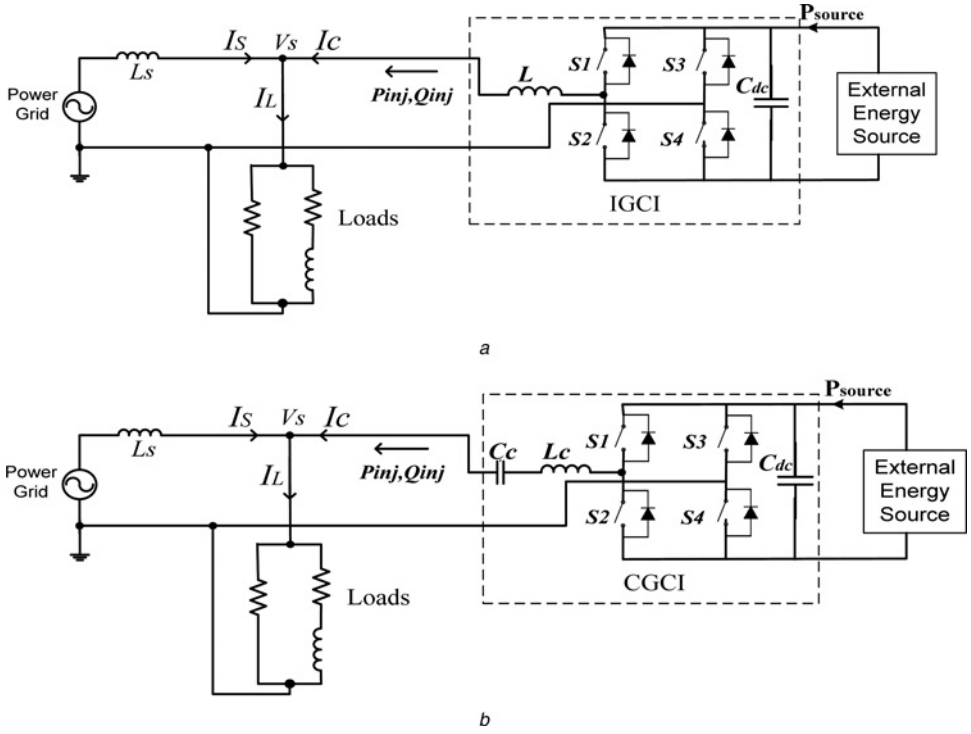

Fig. 1 *Circuit configurations*
a Single-phase IGCI
b Single-phase CGCI

are given in Table 1. The active power and reactive power are each normalised to the defined power base and the corresponding expressions are listed in Table 1. Although, the power base is defined differently for the IGCI and the CGCI, it can be set to the same level by varying the coupling impedance. In the following discussion, normalised values are used to compare the power control capabilities of the two inverters. The output voltage of the inverter is normalised to V_s, the grid voltage at the PCC. When the amplitude of the inverter output voltage is fixed, both the active power flow and the reactive power flow between the inverter and the grid vary according to the phase angle. Five cases are considered within a range of normalised voltage values from 0 to 2; that is, the voltage varies from 0 to double the value of V_s. The variation in the active and reactive power is deduced from the expression in Table 1 and shown in Fig. 2.

Fig. 2 shows that the active power profiles have an odd symmetry for both the IGCI and the CGCI. The active power injected to the grid is zero when the inverter's operational voltage is zero. The active power increases as the inverter voltage increases. The same level of active power can be injected into or absorbed from the grid by varying the phase angle of the inverter voltage. The IGCI injects active power to the grid when the phase angle is positive, and the CGCI injects active power when the phase angle is negative.

However, as shown in Fig. 2*a*, the normalised reactive power equals −1 when the operational voltage of the inverter is 0. This negative value indicates that the injected current from the IGCI is leading the voltage at the PCC. The reactive power of the IGCI takes a positive value only when the inverter voltage is higher

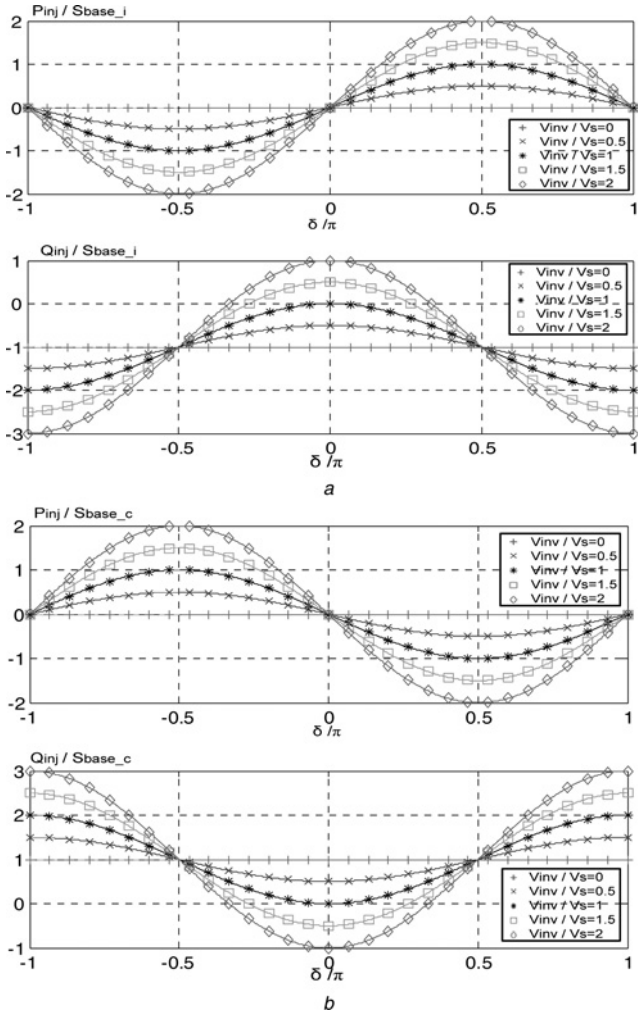

Fig. 2 *Normalised power flow*
a IGCI
b CGCI

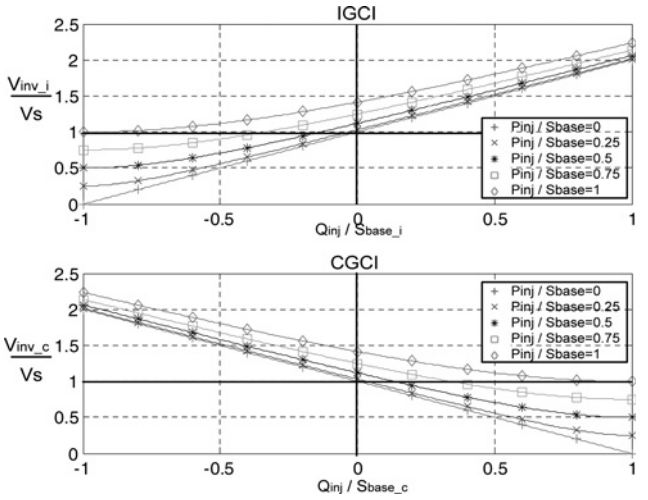

Fig. 3 *Comparison of output voltage values at specific levels of power flow*

than the grid side voltage V_s. However, the normalised reactive power of CGCI equals 1 when its operational voltage is 0, as shown in Fig. 2*b*. A positive value for the reactive power indicates that the injected current from the CGCI is lagging the grid side voltage. If the loading at the PCC is inductive, the power factor can be increased by increasing the positive reactive power.

Once the external sources are connected to the DC-bus, the inverter is able to inject active power to the grid. The output voltage values required for the IGCI and the CGCI to transfer active and reactive power are calculated as follows

$$\frac{V_{\text{inv\_i}}}{V_s} = \sqrt{\left(\frac{P_{\text{inj}}}{S_{\text{base\_i}}}\right)^2 + \left(\frac{Q_{\text{inj}}}{S_{\text{base\_i}}} + 1\right)^2} \tag{6}$$

$$\frac{V_{\text{inv\_c}}}{V_s} = \sqrt{\left(\frac{P_{\text{inj}}}{S_{\text{base\_c}}}\right)^2 + \left(\frac{Q_{\text{inj}}}{S_{\text{base\_c}}} - 1\right)^2} \tag{7}$$

Fig. 3 shows the required operational voltage of the inverter at five active power levels when the normalised reactive power varies from −1 to 1. If the operational voltage of the inverter is lower than V_s, both the IGCI and the CGCI provide reactive power in only one direction, as illustrated in Fig. 3. At the same time, the active power must be lower than the power base.

This paper investigates the use of a grid-connected inverter to inject active power into the grid and compensate reactive power from the inductive load. The proposed inverter type is a CGCI, as this device is capable of providing positive active power and positive reactive power simultaneously when its operational voltage is lower than the grid voltage. As a result, the voltage rating of the inverter remains low and the energy stored in the DC-link is greatly reduced. In the following section, the selection of DC voltage for the CGCI is analysed in detail.

3 DC voltage selection for CGCI

As previously discussed, the power transfer capability of the CGCI varies according to its operational voltage, the maximum amplitude of which is determined by the DC-link voltage of the inverter. The initial cost of the CGCI and its operational losses are lower when the DC-link voltage is reduced. Therefore the selection of an appropriate DC-link voltage for the CGCI is addressed in the system design.

IET Power Electron., 2015, Vol. 8, Iss. 5, pp. 770–782

3.1 Power base and coupling impedance of CGCI

The normalised output voltage of the CGCI is calculated as shown in (7), and its variation in power flow is depicted in three-dimensional (3D) in Fig. 4*a*. The output voltage is zero when the active power is zero and the reactive power is equal to the power base. Fig. 4*b* is the left view of Fig. 4*a*, in which, the horizontal axis indicates variation in reactive power. As shown in Fig. 1*b*, the CGCI operates as a hybrid power filter when no external sources are connected to its DC-bus. In this situation, the output voltage of the inverter varies in linear proportion to the reactive power, as shown in Fig. 4*b*.

When external sources are connected to the DC-bus, the CGCI injects active power into the grid. It can be concluded from Fig. 4*b* that the output voltage of the inverter increases as the active power increases. When the active power transferred is fixed, the required inverter voltage varies according to the reactive power. The active power is transferred at a lower operational voltage when the magnitude of the reactive power is close to that of the power base. Therefore it is most effective to connect the CGCI to the PCC, which requires continues reactive power compensation. To ensure that the CGCI continues to operate at a low DC-link voltage, the power base is chosen according to the average load reactive power at the PCC, which is denoted by $\bar{Q}_{\mathrm{L}}$, as follows

$$S_{\mathrm{base\_c}} = \bar{Q}_{\mathrm{L}} \tag{8}$$

The equivalent capacitance in (1) is deduced by substituting (8) for the power-base definition in Table 1, as follows

$$C = \frac{\bar{Q}_{\mathrm{L}}}{V_{\mathrm{s}}^2 \omega} \tag{9}$$

A coupling inductor is used to limit the high-frequency current ripple, which is $\sim 5\%$ of the coupling capacitor impedance, as shown below

$$\omega L_C = 0.05/(\omega C_C) \tag{10}$$

The coupling impedance can be calculated by combining (1), (9) and (10). Using the resulting coupling impedance value, the reactive power provided by the capacitive-coupling branch is shown to equal the average load reactive power when the output voltage of the inverter is zero. When the load reactive power varies in the vicinity of its average value, a low inverter operational voltage is required to compensate for the reactive power.

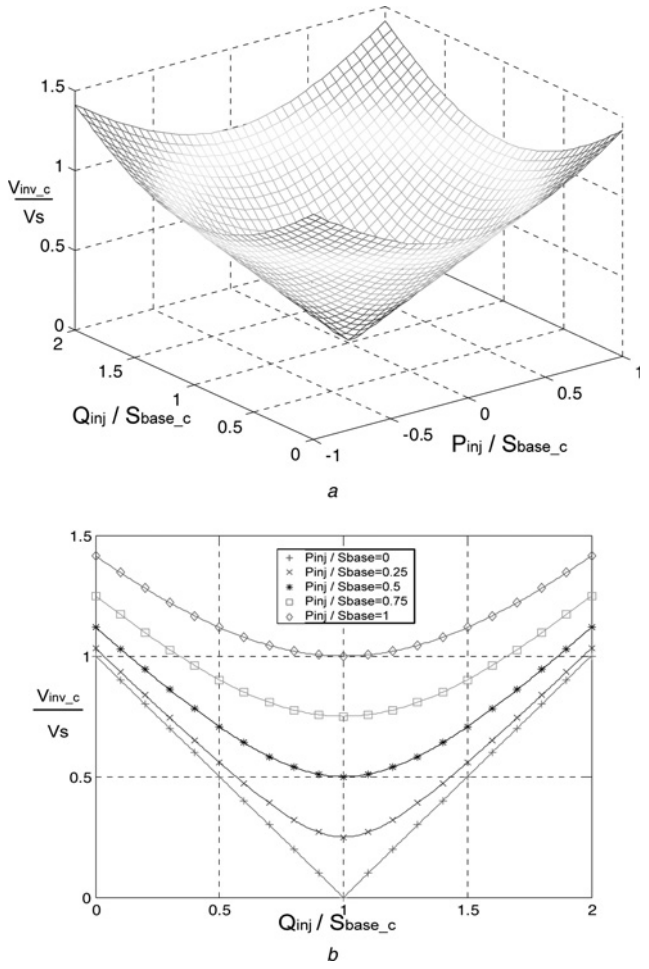

Fig. 4 *Variation in inverter voltage with power*
a 3D view
b Left view

3.2 Selection of DC-link voltage

The DC-link voltage determines the maximum output voltage of the inverter. The achievable power flow range between the inverter and the grid is bounded by the output voltage of the inverter. Fig. 5 provides a view from above of Fig. 4*a*, which illustrates the power flow range bounded by the inverter output voltage. The operational voltage of the inverter at each point can be calculated using (7).

Two operation points are marked in Fig. 5. The same level of active power is injected into the grid at these two points. The reactive power at the two points is denoted by $Q_{\mathrm{inj.up}}$ and $Q_{\mathrm{inj.low}}$, respectively. If the active power is fixed, the range of variation in the reactive power is symmetrical to that of the power base, and varies according to the inverter voltage. The vertical distance between the two points marked in Fig. 5 denotes the reactive

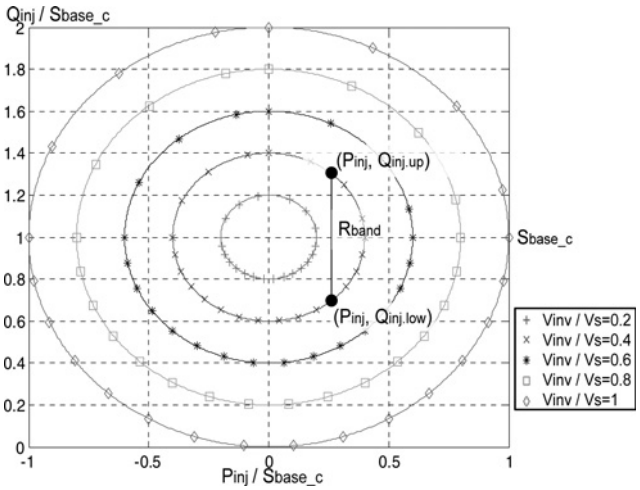

Fig. 5 *Power flow characteristics of CGCI*

Table 2 Parameters determined from the case study

grid-side voltage	220 V
load active power	3.5 kW
power basement, $S_{\mathrm{base\_c}}$	2 kVar
$P_{\mathrm{inj.max}}$	500 W
R_{band}: [$Q_{\mathrm{inj.up}}$, $Q_{\mathrm{inj.low}}$]	0.8: [1.2 kVar, 2.8 kVar]
DC-link voltage	170 V
filter capacitor, C_C	125 μF
filter inductor, L_C	4 mH

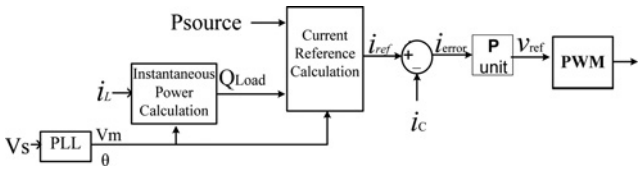

Fig. 6 *Block diagram of CGCI control system*

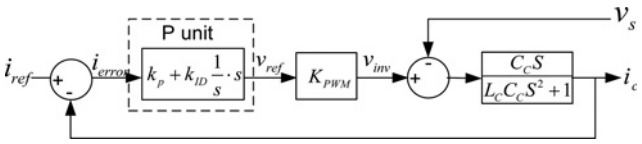

Fig. 7 *Block diagram of CGCI system model*

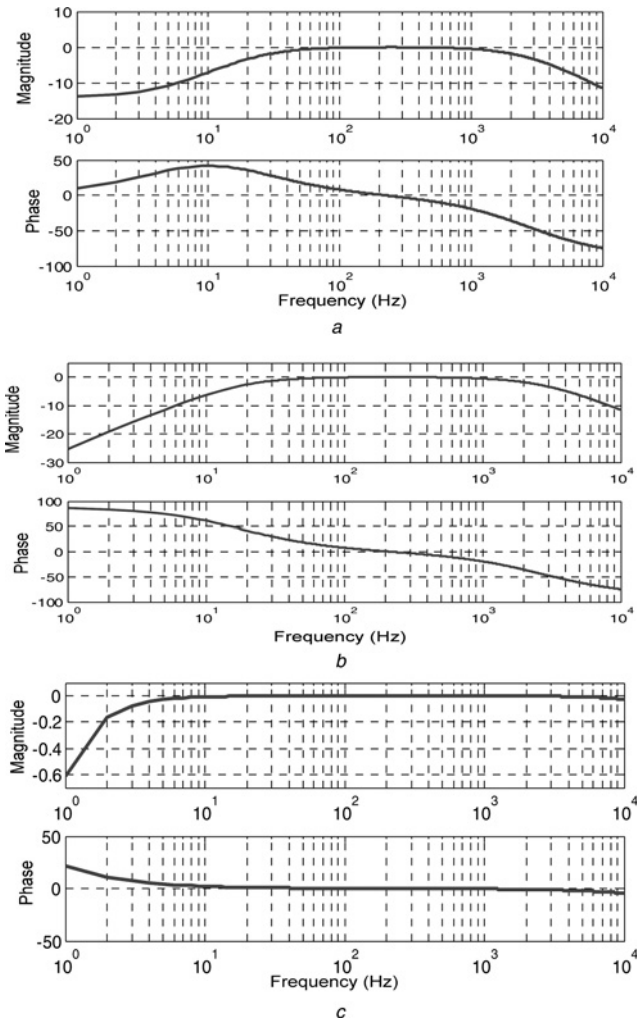

Fig. 8 *Bode diagrams of $G_{iref\_ic}(s)$*

a Using a PI controller
b Using a conventional *P* controller
c Using a ***P***-unit controller

power compensation range, and is expressed as follows

$$R_{\text{band}} = \frac{Q_{\text{inj.up}} - Q_{\text{inj.low}}}{S_{\text{base\_c}}} \tag{11}$$

Owing to the symmetrical properties described, the reactive power

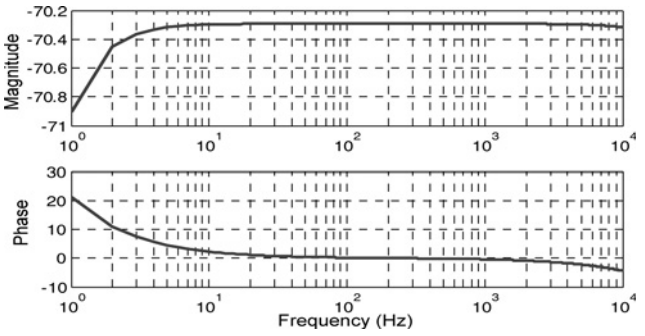

Fig. 9 *Bode diagram of $Z_{vs\_ic}(s)$ using a **P**-unit controller*

Table 3 System settings for the simulation

grid voltage		220 V
switching frequency		10 kHz
K_P, K_{ID}, T_s and T_D		70, 3200, 0.0001 s and 0.01 s
source inductor, L_s		1 mH
linear loads	load 1	15 Ω, 0.12 H, 8 Ω
	load 2	20 Ω, 0.06 H, 10 Ω
	load 3	28 Ω, 0.04 H, 8 Ω

compensation range can be expressed as follows

$$\frac{R_{\text{band}}}{2} = \frac{Q_{\text{inj.up}} - S_{\text{base\_c}}}{S_{\text{base\_c}}} = \frac{S_{\text{base\_c}} - Q_{\text{inj.low}}}{S_{\text{base\_c}}} \tag{12}$$

The output voltage of the inverter corresponding to this reactive power range is deduced by combining (7) and (12), as follows

$$V_{\text{inv}} = V_S\sqrt{\left(\frac{P_{\text{inj}}}{S_{\text{base\_c}}}\right)^2 + \left(\frac{R_{\text{band}}}{2}\right)^2} \tag{13}$$

The maximum active power to be transferred is determined by the external source connected to the CGCI. The output voltage of the inverter is selected according to the required reactive power range when the active power reaches its maximum value. Therefore the DC-link voltage of the CGCI is calculated as follows

$$V_{\text{dc.design}} = M\sqrt{2}V_s\sqrt{\left(\frac{P_{\text{inj.max}}}{S_{\text{base\_c}}}\right)^2 + \left(\frac{R_{\text{band}}}{2}\right)^2} \tag{14}$$

The coefficient M is introduced to provide redundancy in the DC-link voltage design. When a safe margin of 15% is selected, M equals 1.15. A wider compensation range requires a higher voltage.

One case is considered here in which the apparent power of the load at the PCC is set to 1, with a power factor of 0.85. Assuming that the load is linear and the distortion power is ignored, the load active power is normalised to 0.85, and the reactive power is ~0.52 in per-unit form. The value of $S_{\text{base\_c}}$ is established from the reactive power, giving 0.5 in per unit form for this case study. The following considerations should be taken into account.

- *Reactive power compensation only*. If no external sources are connected to the CGCI, the CGCI operates as a hybrid power filter when compensating the reactive power. The DC-link voltage is determined by the required reactive power range, and $P_{\text{inj.max}}$ is zero.
- *Active power control with fixed reactive power*. After an external source has been connected, active power is injected into the DC bus. The DC-link voltage varies according to $P_{\text{inj.max}}$, and R_{band} is set to zero if the reactive power is fixed at $S_{\text{base\_c}}$. Assuming that the penetration rate of the active power at the grid side is lower than 15%, the highest value of the active power, $P_{\text{inj.max}}$ is ~0.26, as calculated from the selected $S_{\text{base\_c}}$. The corresponding DC-link voltage is 0.42 Vs.

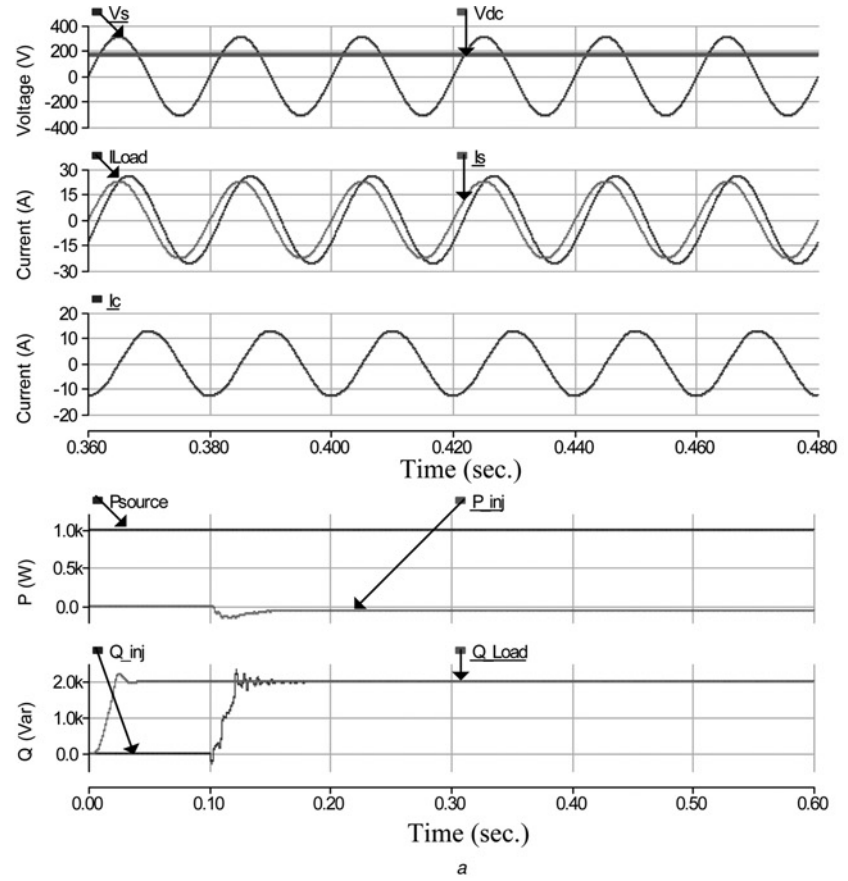

a

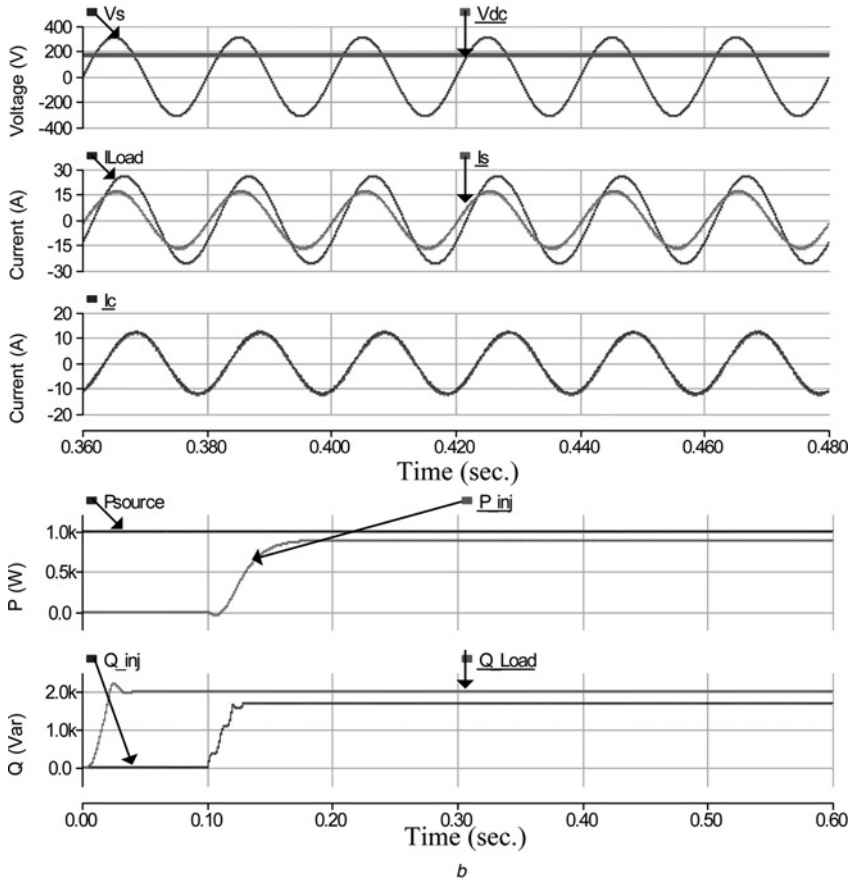

b

Fig. 10 *Simulation results*

a With a *PI* controller
b With a *P* controller
c With a ***P***-unit controller

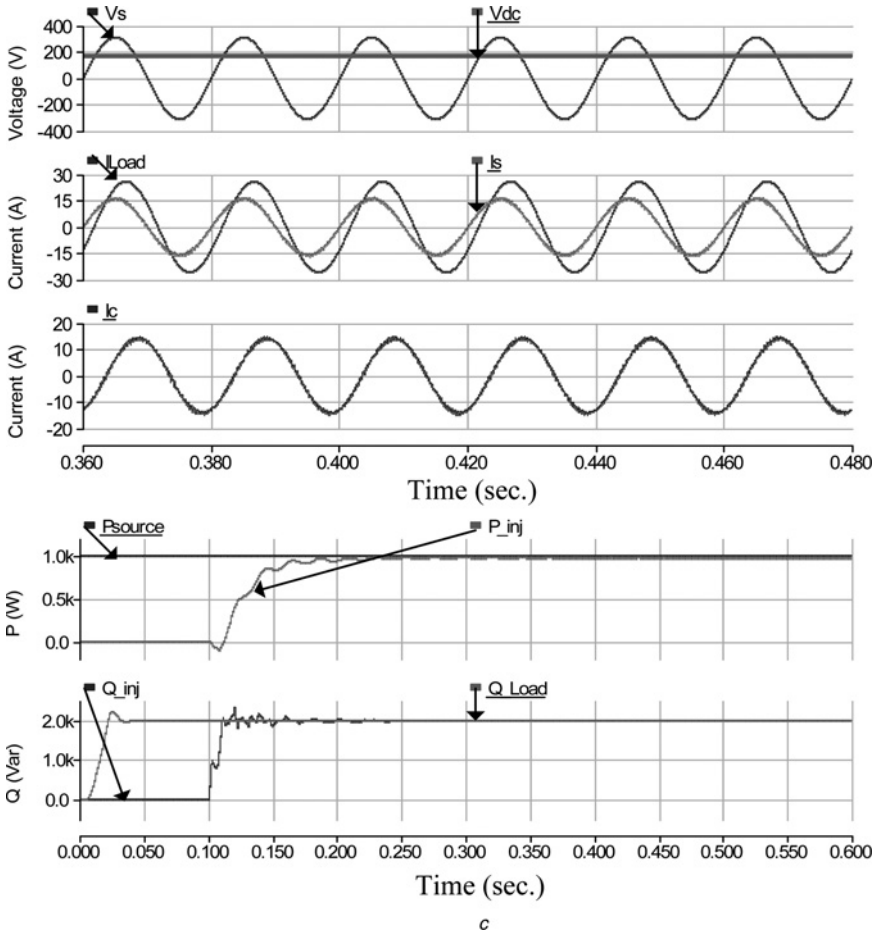

c

Fig. 10 *Continued*

Table 4 Comparison of current controllers

	Current RMS, A	Current THD, %	Active power, W	Reactive power, Var	Power factor
load	18.4	0.00	3483	2004	0.87
PI ($k_p = 70$, $k_i = 2000$)	16.06	0.87	3533	5.61	0.990
P ($k_p = 70$)	11.95	0.92	2599	327	0.992
P-unit ($k_p = 70$, $k_{ID} = 3200$)	11.48	1.50	2516	10.06	0.990

• *Active and reactive power control*. When the maximum value of the active power, $P_{inj.max}$, is ~ 0.26, the reactive power compensation range, R_{band}, is set to 0.8 to ensure that the CGCI can cope with the variation in load. This increases the DC-link voltage to 0.77 Vs.

It is assumed that the load active power is 3.5 kW and S_{base_c} is 2 kVar. The system parameters are determined from the results of the case study and are listed in Table 2. The required DC-link voltage is 170 V. To achieve the same power range, the DC-link voltage of the IGCI must be higher than 1.414 Vs, that is, ~ 340 V or higher. At this DC voltage, the energy stored in the DC capacitor of the IGCI is four times greater than that stored in the CGCI.

3.3 Summary

The selected coupling impedance and DC-link voltage values are presented in this section. The proposed design enables the CGCI to achieve the following goals simultaneously at a low DC-link voltage.

• Injection of active power from the external source to the grid when the reactive power varies within the compensation range.

• Improvement of the power factor at the grid side.

The control system of the CGCI is described in details in the following section.

4 CGCI control systems

Fig. 6 shows the overall control blocks of the CGCI. The single-phase instantaneous reactive power (IRP) theory is used to calculate the instantaneous load power and the current reference. It is assumed that the loads are linear. The reactive power of the loads is calculated as follows

$$Q_L = v_m i_L \cos\theta - v_m i_{Ld} \sin\theta \tag{15}$$

In (15), i_L is the load current and i_{Ld} is its delay for one-quarter of a cycle. The reference currents are calculated as follows

$$i_{ref} = \frac{1}{v_m^2}\begin{bmatrix} v_m \sin\theta & v_m \cos\theta \end{bmatrix}\begin{bmatrix} P_{source} \\ Q_L \end{bmatrix} \tag{16}$$

The active power injected into the grid, which is usually determined by the external energy sources, is set manually, as shown in Fig. 6. The reference currents are compared with the output current of the CGCI. The current errors are sent to a ***P***-unit, the output of which is the pulse-width modulation (PWM) reference. The ***P***-unit is described in detail later this section.

The current controller of the CGCI is modelled, and a block diagram of the CGCI system is provided in Fig. 7. K_{PWM} is the inverter gain, which is regarded as unity when the control system delay is ignored.

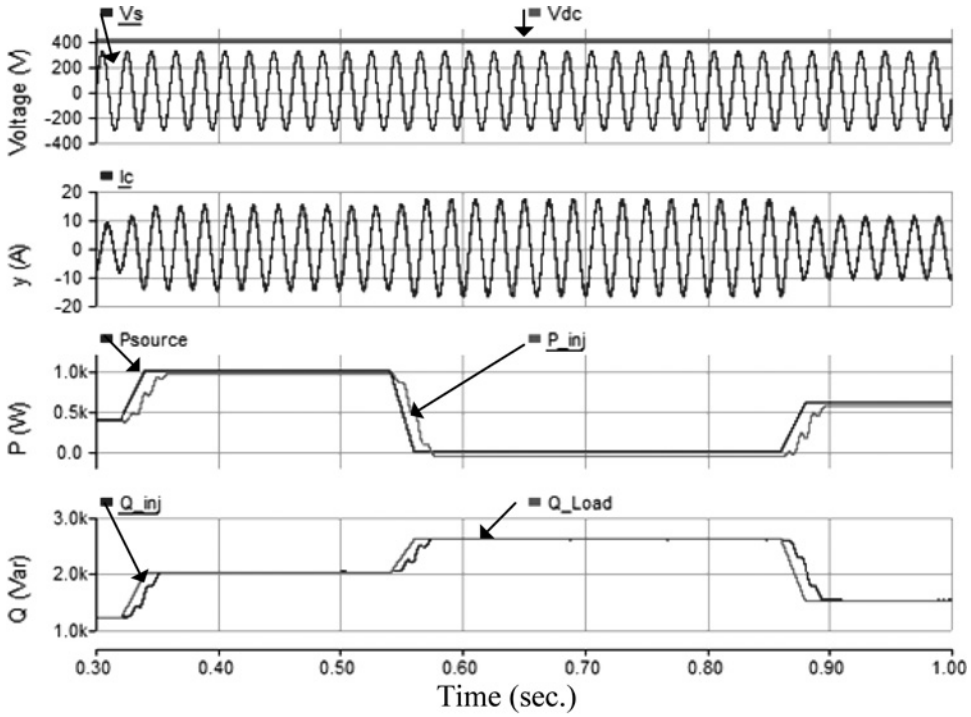

a

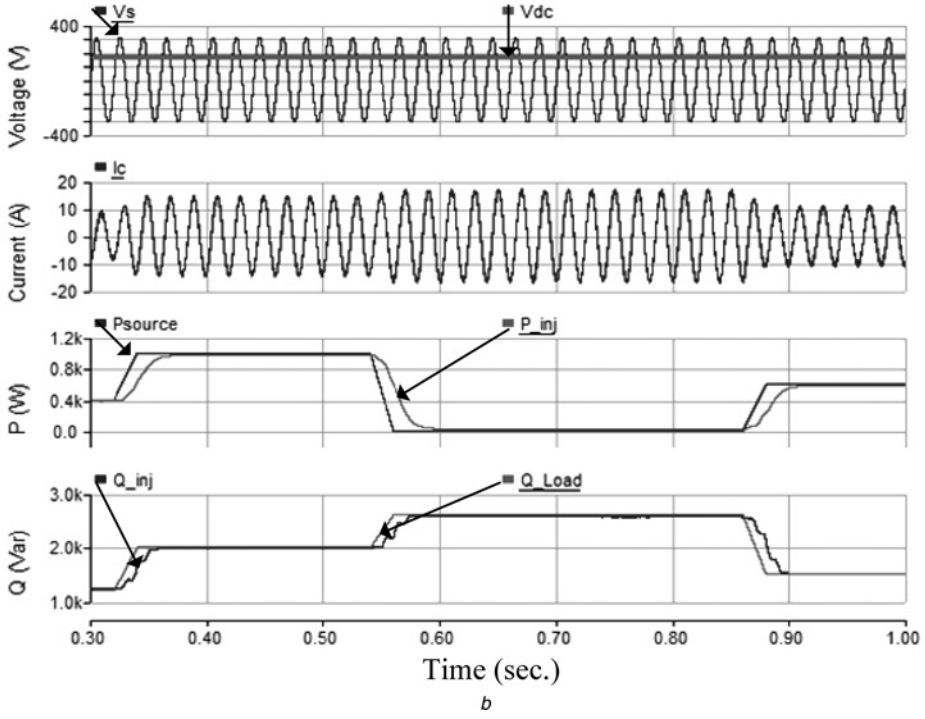

b

Fig. 11 *Grid-connected inverters used to achieve dynamic power transfer*

a IGCI
b CGCI

The corresponding transfer function is deduced as follows

$$\begin{aligned} I_c(s) &= G_{\text{iref\_ic}}(s)I_{\text{ref}}(s) - Z_{vs\_ic}(s)V_{\text{s}}(s) \\ &= \frac{P \cdot C_C \cdot k_{\text{PWM}} \cdot s}{L_C C_C s^2 + P \cdot C_C \cdot k_{\text{PWM}} \cdot s + 1} I_{\text{ref}}(s) \\ &\quad - \frac{C_C \cdot s}{L_C C_C s^2 + P \cdot C_C \cdot k_{\text{PWM}} \cdot s + 1} V_{\text{s}}(s) \end{aligned} \tag{17}$$

The control system of an IGCI usually sends current tracking errors to a proportional–integral (PI) unit to generate a PWM reference [37]. However, if a PI unit is used in the control system of the CGCI, P in (17) is replaced by $(k_p + k_i/\text{s})$. When $k_p = 70$, $k_i = 2000$ and the parameters are as listed in Table 2, the system response is as shown in Fig. 8*a*. If only proportional (P) control is used, the system response is as shown in Fig. 8*b*, where $k_{\text{p}} = 70$. It can be concluded that the output current of the CGCI is unable to track the reference when a PI controller or a P

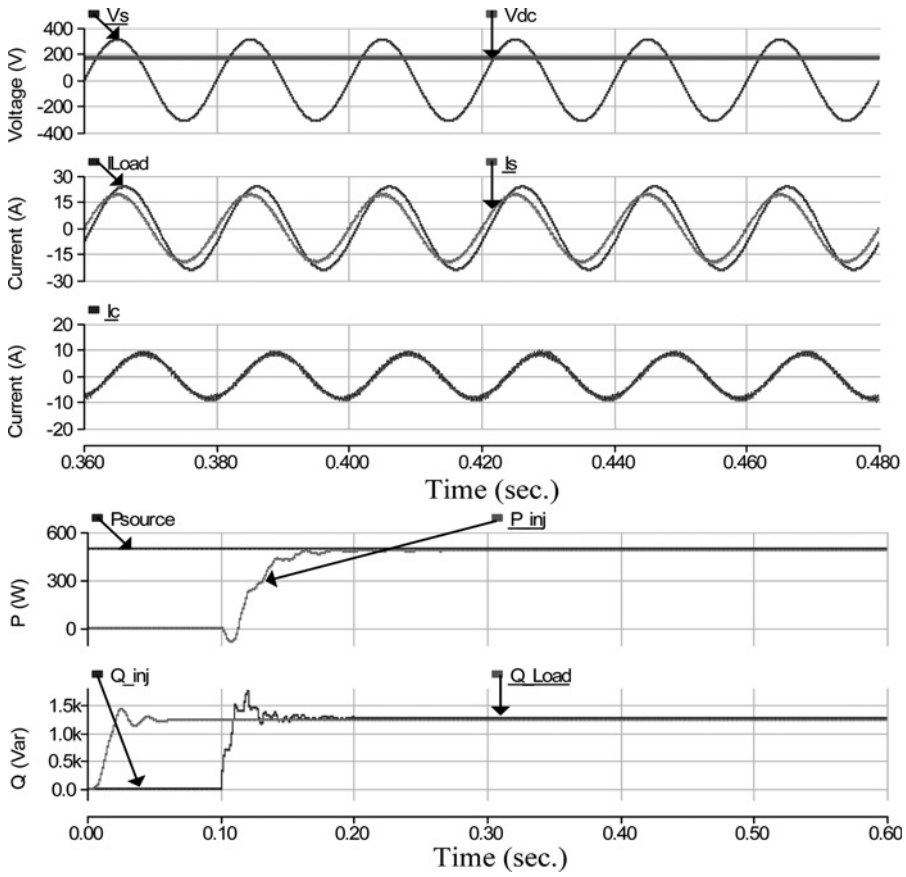

Fig. 12 *Current waveform and DC-link voltage for load 1*

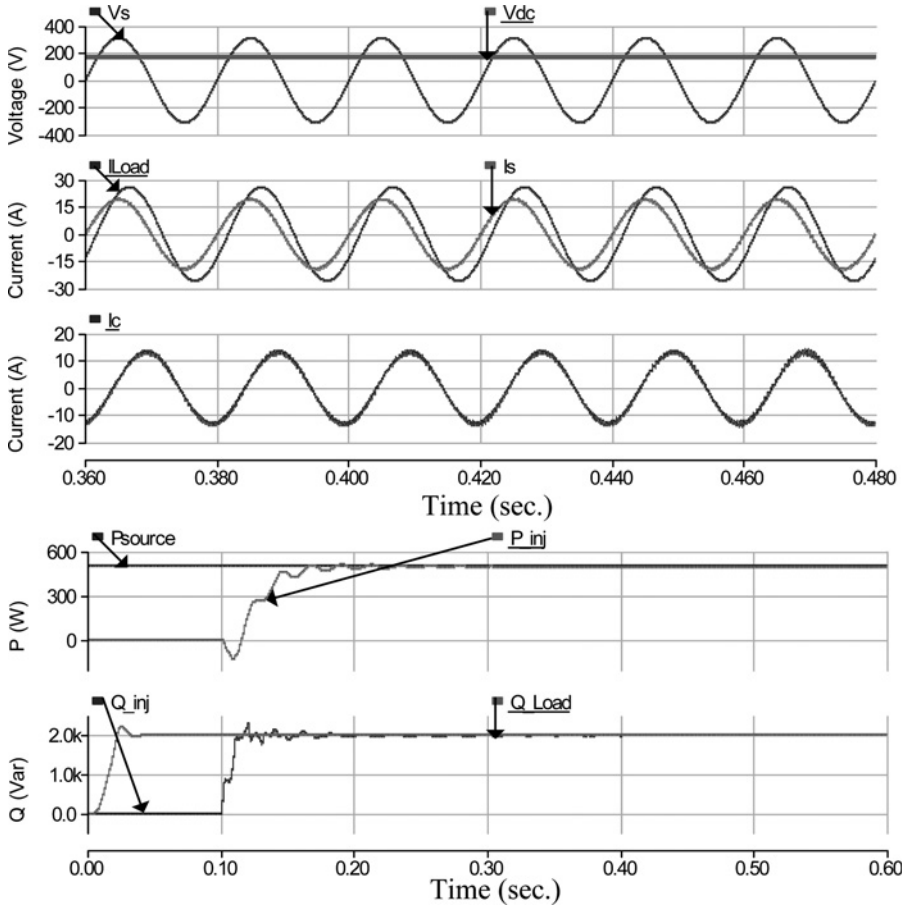

Fig. 13 *Current waveform and DC-link voltage for load 2*

IET Power Electron., 2015, Vol. 8, Iss. 5, pp. 770–782

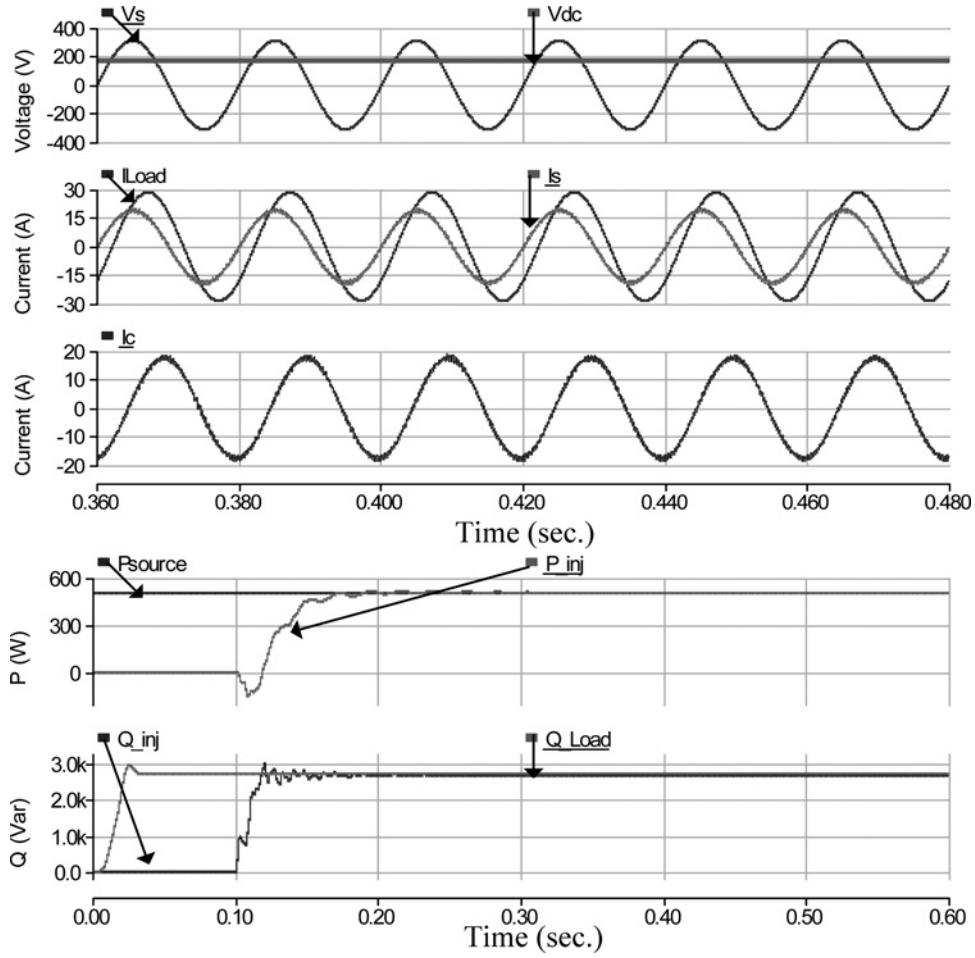

Fig. 14 *Current waveform and DC-link voltage for load 3*

controller is used. In these cases, the system performance is poor. Fig. 7 shows the new control block proposed in this paper, which has the following formula

$$v_{\text{ref}} = k_{\text{p}} \cdot i_{\text{error}} + k_{\text{ID}} \frac{d\left(\int_0^t i_{\text{error}} \text{d}t\right)}{\text{d}t} \tag{18}$$

When $k_{\text{p}} = 70$ and $k_{\text{ID}} = 3200$, the total gain of the ***P***-unit is 3270. The corresponding system response is depicted in Fig. 8*c*, which shows that the current tracking performance is greatly improved.

In the continuous-time system model, the performance of the proposed ***P***-unit is the same as that of a pure proportional controller. However, the sole application of proportional gain causes over-modulation and system instability. When the control algorithm is implemented in a digital controller, the discrete-time control block is deduced as follows

$$\begin{aligned} v_{\text{ref}}[n] &= k_{\text{p}} \cdot i_{\text{error}}[n] + k_{\text{ID}} \\ &\quad \times \frac{T_{\text{s}}\left(\sum_{k=0}^{t/T_{\text{s}}} i_{\text{error}}[n-k] - \sum_{k=0}^{(t-T_{\text{D}})/T_{\text{s}}} i_{\text{error}}[n-k]\right)}{T_{\text{D}}} \\ &= k_{\text{p}} \cdot i_{\text{error}}[n] + k_{\text{ID}} \cdot \frac{T_{\text{s}}}{T_{\text{D}}} \sum_{k=0}^{T_{\text{D}}/T_{\text{s}}} i_{\text{error}}[n-k] \end{aligned} \tag{19}$$

In (19), T_{s} is the sampling period of the digital controller and T_{D} is the time-constant used in the differential part of the equation.

The system response to grid-side voltage is shown in Fig. 9. It is evident from Fig. 9 that the CGCI does not amplify harmonic distortion in the grid-side voltage. Therefore the LC branch of the CGCI control system is not responsible for the unwanted oscillations.

Table 5 Simulation results verifying the reactive power range

	Current RMS, A	Current THD, %	Active power, W	Reactive power, Var	Power factor
load 1	16.9	0.00	3487	1228	0.943
source 1	13.67	1.24	3005	−30	1.000
load 2	18.4	0.00	3483	2004	0.87
source 2	13.6	1.83	2995	9.26	1.000
load 3	20.2	0.00	3473	2741	0.785
source 3	13.6	1.91	2976	40	1.000

Table 6 Experimental system parameters

grid voltage V_{s}		55 V
DC bus voltage		39 V
coupling capacitor		130 μF
coupling inductor		3.5 mH
switching frequency		10 kHz
loads	load 1	0.06 H, 15 Ω, 100 Ω
	load 2	0.06 H, 10 Ω, 100 Ω
	load 3	0.06 H, 5 Ω, 60 Ω

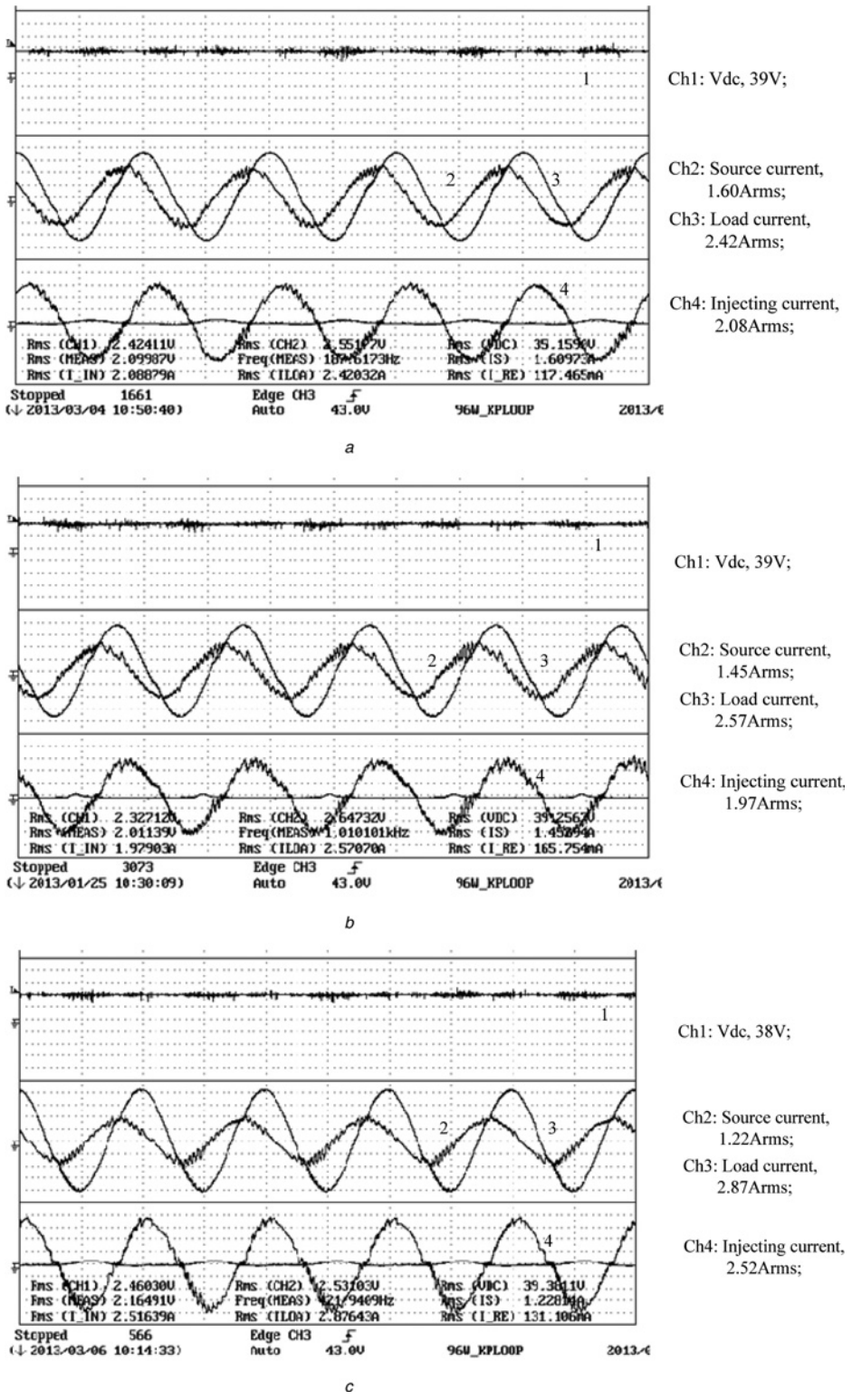

Fig. 15 *Results of experiment conducted to verify the reactive power compensation range*

a Load 1
b Load 2
c Load 3

5 Simulation results

The simulation models are built using PSCAD/EMTDC software. The system configuration is given in Fig. 1*b*. The external energy source is modelled as a DC source, and its injection of active power to the DC-bus is determined by the setting in simulation. The case study described in Table 2 is used in the simulation. Additional settings for the simulation are listed in Table 3.

5.1 Comparison of current control units

The three current controllers PI, *P* and ***P***-unit are compared in Section 4 using Bode diagrams deduced from the system transfer function. Each of the three controllers is used in the simulations to control the CGCI. The load reactive power is equal to the selected power base. The active power to be transferred is set to 1 kW. The results obtained are given in Fig. 10 and Table 4. It can be

IET Power Electron., 2015, Vol. 8, Iss. 5, pp. 770–782

Table 7 Results of experiments conducted to verify the reactive power range

	Current RMS, A	Active power, W	Reactive power, Var	Power factor
load 1	2.50	93	81	0.76
source under load 1	1.60	76	−28	0.95
load 2	2.57	90	117	0.63
source under load 2	1.45	70	−7	0.98
load 3	2.87	95	150	0.58
source under load 3	1.22	75	−6	0.98

concluded that the proposed ***P***-unit controller achieves the best performances in transferring the required power to the grid. The PI controller fails to transfer active power to the grid. The steady state error is high when the *P* controller is used.

5.2 Comparison of IGCI and CGCI

In this section, the performance of the IGCI is compared with that of the CGCI. The DC-link voltage of the IGCI is 400 V and the DC-link voltage of the CGCI is 170 V. The results of the simulation are shown in Fig. 11. The two grid-connected inverters are tested in conditions of dynamic change in active power and reactive power. The results indicate that both inverters are able to transfer the required active power and reactive power to the power grid. However, the operational voltage of the CGCI is much lower than that of the IGCI.

5.3 Verification of the power flow control range of the CGCI

Three groups of linear loads are tested to verify the power control range of the CGCI when its DC-link voltage is set to 170 V. The selected reactive power range is given in Table 2. The load settings used in the simulation are listed in Table 3. The simulation results are illustrated in Figs. 12–14. In Fig. 12, the load reactive power is shown to approach the lower boundary. Fig. 13 shows the magnitude of the load reactive power to be closer to that of the power base, and in Fig. 14 the load reactive power is shown to approach the upper boundary. In all three cases, the active power to be transferred is 500 W. The active and reactive power values at the load side and the grid side are listed in Table 5. The results indicate that active power from the external sources can be injected into the grid when the reactive power is within the designated range. The CGCI is able to transfer active power and reactive power simultaneously at a DC-link voltage of approximately half the peak grid voltage. In addition, the distortion in the current profile is still inside the acceptable range as illustrated in the simulation results.

6 Experimental results

A lab-scale prototype is built, and the CGCI system is configured as that in Fig. 1*b*. The control platform is based on the DSP TMS320F2812. The system parameters are listed in Table 6. The grid-side voltage is reduced to 55 V because of the limitations of the laboratory setting. When the active power is 20 W and the reactive power compensation range is [82 and 178 Var], the DC-link voltage is 39 V. The required DC-link voltage of the IGCI is higher than 70 V. Linear loads are used to verify the reactive power compensation range of the selected DC voltage. Three groups of loads are also tested experimentally and the results are provided in Fig. 15 and Table 7, show the CGCI is capable of controlling active and reactive power flows simultaneously. The previously required power control range is also achieved in the experiment. However, the measured THD of the source current, as shown in Fig. 15*b* is 6.16%. The greater distortion recorded in the experiment is chiefly because of the noise introduced in the signal-conditioning circuits and the truncation errors generated by the fixed-point DSP.

7 Conclusions

In this paper, a CGCI was proposed as a low-cost alternative to conventional IGCIs. The power flow control characteristics of the two types of grid-connected inverter are analysed and compared. We can conclude that the CGCI is able to transfer active power with a much lower operational voltage when the magnitude of its output reactive power is close to that of its power base. As a result, the initial cost, the operational losses and the energy stored in the DC bus are all reduced in comparison with those of the conventional IGCI. Furthermore, a DC voltage selection method and a novel ***P***-unit current controller are proposed for use with the CGCI. The results of simulations and experiments verified the feasibility of the CGCI topology and the effectiveness of the control method.

8 Acknowledgments

The authors would like to thank the Science and Development Fund, Macao SAR Government with the project (072/2012/A3), University of Macau with the project (MYRG 135 (Y2-L2)-FST11-DNY) for their financial support.

9 References

1 Guerrero, J.M., Blaabjerg, F., Zhelev, T., *et al.*: 'Distributed generation: toward a new energy paradigm', *IEEE Ind. Electron. Mag.*, 2010, **4**, (2), pp. 52–64
2 Ahmed, M.E.-S., Orabi, M., AbdelRahim, O.M.: 'Two-stage micro-grid inverter with high-voltage gain for photovoltaic applications', *IET Power Electron.*, 2013, **6**, (9), pp. 1812–1821
3 de Almeida, P.M., Duarte, J.L., Ribeiro, P.F., Barbosa, P.G.: 'Repetitive controller for improving grid-connected photovoltaic systems', *IET Power Electron.*, 2014, **7**, (6), pp. 1466–1474
4 Reigosa, D., Briz, F., Blanco, C., Garcia, P.: 'Active islanding detection for multiple parallel-connected inverter-based distributed generators using high frequency signal injection', *IEEE Trans. Power Electron.*, 2014, **29**, (3), pp. 1192–1199
5 Guerrero, J.M., Poh, C.L., Lee, T.L., Chandorkar, M.: 'Advanced control architectures for intelligent microgrids – Part II: power quality, energy storage, and AC/DC microgrids', *IEEE Trans. Ind. Electron.*, 2013, **60**, (4), pp. 1263–1270
6 Wai, R.J., Lin, C.Y., Wu, W.C., Huang, H.N.: 'Design of backstepping control for high-performance inverter with stand-alone and grid-connected power supply modes', *IET Power Electron.*, 2012, **6**, (4), pp. 752–762
7 Guo, Z., Sha, D., Liao, X.: 'Voltage magnitude and frequency control of three-phase voltage source inverter for seamless transfer', *IET Power Electron.*, 2014, **7**, (1), pp. 200–208
8 Chang, C.H., Wu, F.Y., Chen, Y.M.: 'Modularized bidirectional grid-connected inverter with constant-frequency asynchronous sigma-delta modulation', *IEEE. Trans. Ind. Electron.*, 2012, **59**, (11), pp. 4088–4100
9 Balthandayuthapani, S., Edrington, C.S., Henry, S.D., Cao, J.: 'Analysis and control of a photovoltaic system: application to a high-penetration case study', *IEEE Syst. J.*, 2012, **6**, (2), pp. 213–219
10 Xiao, H., Xie, S., Chen, Y., Huang, R.: 'An optimized transformerless photovoltaic grid-connected inverter', *IEEE Trans. Ind. Electron.*, 2011, **58**, (5), pp. 1887–1895
11 Singh, B., Saha, R., Chandra, A., Al-Haddad, K.: 'Static synchronous compensator (STATCOM): a review', *IET Power Electron.*, 2009, **2**, (4), pp. 297–324
12 She, X., Huang, A.Q., Wang, F., Burgos, R.: 'Wind energy system with integrated functions of active power transfer, reactive power compensation and voltage conversion', *IEEE Trans. Ind. Electron.*, 2013, **60**, (10), pp. 4512–4522
13 Rajendran, S., Govindarajan, U., Reuben, A.B., Srinivasan, A.: 'Shunt reactive VAR compensator for grid-connected induction generator in wind energy conversion systems', *IET Power Electron.*, 2013, **6**, (9), pp. 1872–1883
14 Dasgupta, S., Mohan, S.N., Sahoo, S.K., Panda, S.K.: 'A Lyapunov function based current controller to control active and reactive power flow in a three phase grid connected PV inverter under generalized grid voltage conditions'. Proc. Eighth Int. Conf. Power Electronics, Jeju, Korea, 2011, pp. 1110–1117
15 Bonfiglio, A., Brignone, M., Delfino, F., Procopio, R.: 'Optimal control and operation of grid-connected photovoltaic production units for voltage support in medium-voltage networks', *IEEE Trans. Sustain. Energy*, 2014, **5**, (1), pp. 254–263
16 Zeng, Z., Zhao, R.X., Yang, H.: 'Coordinated control of multi-functional grid-tied inverters using conductance and susceptance limitation', *IET Power Electron.*, 2014, **7**, (7), pp. 1821–1831

17 Bojoi, R.I., Limongi, L.R., Roiu, D., Tenconi, A.: 'Enhanced power quality control strategy for single-phase inverters in distributed generation systems', *IEEE Trans. Power Electron.*, 2011, **26**, (3), pp. 798–806
18 Dasgupta, S., Sahoo, S.K., Panda, S.K.: 'Single-phase inverter control techniques for interfacing renewable energy sources with microgrid – Part I: Parallel-connected inverter topology with active and reactive power flow control along with grid current shaping', *IEEE Trans. Power Electron.*, 2011, **26**, (3), pp. 717–731
19 Zhang, Q.C., Hornik, T.: 'Cascaded current-voltage control to improve the power quality for a grid-connected inverter with a local load', *IEEE Trans. Ind. Electron.*, 2013, **60**, (4), pp. 1344–1355
20 Chang, C.H., Lin, Y.H., Chen, Y.M., Chang, Y.R.: 'Simplified reactive power control for single-phase grid-connected photovoltaic inverters', *IEEE Trans. Ind. Electron.*, 2014, **61**, (5), pp. 2286–2296
21 Sun, P., Liu, C., Lai, J.S., Chen, C.L.: 'Grid-tie control of cascade dual-buck inverter with wide-range power flow capability for renewable energy applications', *IEEE Trans. Power Electron.*, 2012, **27**, (4), pp. 1839–1849
22 Liu, L., Li, H., Wu, Z., Zhou, Y.: 'A cascaded photovoltaic system integrating segmented energy storages with self-regulating power allocation control and wide range reactive power compensation', *IEEE Trans. Power Electron.*, 2011, **26**, (12), pp. 3545–3559
23 Park, S.Y., Chen, C.L., Lai, J.: 'A wide-range active and reactive power flow controller for a solid oxide fuel cell power conditioning system', *IEEE Trans. Power Electron.*, 2009, **23**, (6), pp. 2703–2710
24 Vijayakumar, K., Kumaresan, N., Gounden, N.G.A., Tennakoon, S.B.: 'Real and reactive power control of hybrid excited wind-driven grid-connected doubly fed induction generators', *IET Power Electron.*, 2013, **6**, (6), pp. 1197–1208
25 Litran, S.P., Salmeron, P.: 'Reference voltage optimization of a hybrid filter for nonlinear load compensation', *IEEE Trans. Ind. Electron.*, 2014, **61**, (6), pp. 2648–2654
26 Rahmani, S., Hamadi, A., Al-Haddad, K., Dessaint, L.A.: 'A combination of shunt hybrid power filter and thyristor-controlled reactor for power quality', *IEEE Trans. Ind. Electron.*, 2014, **61**, (5), pp. 2152–2164
27 Akagi, H., Inzunza, R.: 'A 6.6-kV transformerless shunt hybrid active filter for installation on a power distribution system', *IEEE Trans. Power Electron.*, 2005, **20**, (4), pp. 893–900
28 Lam, C.S., Wong, M.C., Han, Y.D.: 'Hysteresis current control of hybrid active power filters', *IET Power Electron.*, 2012, **5**, (7), pp. 1175–1187
29 Zhang, W.C., Dai, N.Y., Wong, M.C., Wong, C.K.: 'Capacitive-coupled grid-connected inverter with active power injection ability'. Proc. of Seventh Int. Power Electronics and Motion Control Conf. (IPEMC), Harbin, China, June 2012, pp. 1639–1645
30 Lam, C.S., Cui, X.X., Choi, W.H., Wong, M.C., Han, Y.D.: 'Minimum inverter capacity design for LC-hybrid active power filters in three-phase four-wire distribution systems', *IET Power Electron.*, 2012, **5**, (7), pp. 956–968
31 Yingdong, W.: 'Research on control of comprehensive compensation for traction substations based on the STATCOM technology', PhD thesis, Tsinghua University, 2009
32 http://www.alibaba.com/product-detail/Power-Quality-Power-Distribution-Reactive-Power_1962923292.html?s=p, accessed September 2014
33 http://www.alibaba.com/product-detail/Three-phase-active-power-filter-for_1849805308.html, accessed September 2014
34 Akagi, H., Isozaki, K.: 'A hybrid active filter for a three-phase 12-pulse diode rectifier used as the front end of a medium-voltage motor drive', *IEEE Trans. Power Electron.*, 2012, **27**, (1), pp. 69–77
35 Guerrero, J.M., Matas, J., Vicua, L.G., Castilla, M., Miret, J.: 'Wireless-control strategy for parallel operation of distributed-generation inverters', *IEEE Trans. Ind. Electron.*, 2006, **53**, (5), pp. 1461–1470
36 Guerrero, J.M., Chandorkar, M., Lee, T., Loh, P.C.: 'Advanced control architectures for Intelligent microgrids – Part I: decentralized and hierarchical control', *IEEE Trans. Ind. Electron.*, 2013, **60**, (40), pp. 1254–1262
37 Yang, S., Lei, Q., Peng, F.Z., Qian, Z.: 'A robust control scheme for grid-connected voltage-source inverters', *IEEE Trans. Ind. Electron.*, 2011, **58**, (1), pp. 202–212